

AD-753 392

A LABORATORY METHOD FOR THERMAL
FRACTURE OF GRAPHITE

Hans U. Eckert

Aerospace Corporation

Prepared for:

Space and Missile Systems Organization

31 October 1972

DISTRIBUTED BY:

NTIS

National Technical Information Service
U. S. DEPARTMENT OF COMMERCE

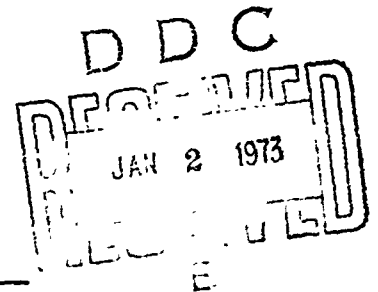
5285 Port Royal Road, Springfield Va 22151

AD753392

A Laboratory Method for Thermal Fracture of Graphite

Prepared by H. U. ECKERT
Plasma Research Laboratory
Laboratory Operations

72 OCT 31



Development Operations
THE AEROSPACE CORPORATION

Prepared for SPACE AND MISSILE SYSTEMS ORGANIZATION
AIR FORCE SYSTEMS COMMAND
LOS ANGELES AIR FORCE STATION
Los Angeles California

NATIONAL TECHNICAL
INFORMATION SERVICE

APPROVED FOR PUBLIC RELEASE DISTRIBUTION UNLIMITED

UNCLASSIFIED

Security Classification

DOCUMENT CONTROL DATA - R & D		
<i>(Security classification of title, body of abstract and indexing annotation must be entered when the overall report is classified)</i>		
1. ORIGINATING ACTIVITY (Corporate author)		2a. REPORT SECURITY CLASSIFICATION
The Aerospace Corporation El Segundo, California		Unclassified
		2b. GROUP
3. REPORT TITLE		
A LABORATORY METHOD FOR THERMAL FRACTURE OF GRAPHITE		
4. DESCRIPTIVE NOTES (Type of report and inclusive dates)		
5. AUTHOR(S) (First name, middle initial, last name)		
Hans U. Eckert		
6. REPORT DATE	7a. TOTAL NO. OF PAGES	7b. NO. OF REFS
72 OCT-31	41	5
8a. CONTRACT OR GRANT NO.	9a. ORIGINATOR'S REPORT NUMBER(S)	
F04701-72-C-0073	TR-0073(3450-76)-1	
b. PROJECT NO.		
c.	9b. OTHER REPORT NO(S) (Any other numbers that may be assigned this report)	
d.	SAMSO-TR-72-275	
10. DISTRIBUTION STATEMENT		
Approved for public release; distribution unlimited		Details of illustrations in this document may be better studied on microfiche.
11. SUPPLEMENTARY NOTES	12. SPONSORING MILITARY ACTIVITY	
	Space and Missile Systems Organization Air Force Systems Command Los Angeles, California	
13. ABSTRACT		
<p>Development of a method for producing thermal stress failure in ATJ-S graphite and the initial results are described. Test specimens are 10-cm-long hollow cylinders with outer and inner radii of 1.9 and 0.4 cm, respectively. The outside is heated by induction at a frequency of 1.4 MHz by a 100-kW power oscillator; the inside is kept below 100°C by forcing water at a rate of 5 gpm through the copper-coated bore. A special lead soldering technique has been developed to fasten the coolant ducts to the specimen. The inductor coil is protected by an oil bath against heat and electric breakdown. From the recorded rise in cooling water temperature, radial heat fluxes through the specimen at fracture have been determined to be 38 kW. The surface temperature at fracture has been measured pyrometrically to be ~1700°C. The mean radial temperature gradient at the section where fracture occurs is ~1050°C/cm, which comes close to theoretical predictions. Fast heating seems to produce fracture at lower power. Recommendations are given for improving and extending the measurements. A method is developed for calculating radial temperature distributions that takes into account effects of heater frequency, temperature dependence of thermal conductivity, and surface radiation. Sample calculations for ATJ graphite show nearly linear temperature variations. Therefore, the mean gradient obtained from the measurements can be expected to approximate values of the local temperature gradients.</p>		

UNCLASSIFIED

Security Classification

14

KEY WORDS

Graphite
Thermal Fracture
Induction Heating

Distribution Statement (Continued)

Abstract (Continued)

Th
UNCLASSIFIED

Security Classification

Air Force Report No.
SAMSO-TR-72-275

Aerospace Report No.
TR-0073(3450-76)-1

A LABORATORY METHOD FOR THERMAL
FRACTURE OF GRAPHITE

Prepared by
H. U. Eckert
Plasma Research Laboratory
Laboratory Operations

72 OCT 31

Development Operations
THE AEROSPACE CORPORATION

Prepared for
SPACE AND MISSILE SYSTEMS ORGANIZATION
AIR FORCE SYSTEMS COMMAND
LOS ANGELES AIR FORCE STATION
Los Angeles, California

Approved for public release;
distribution unlimited

IC

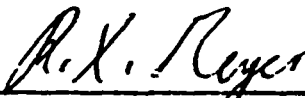
FOREWORD

This report is published by The Aerospace Corporation, El Segundo, California, under Air Force Contract No. F04701-72-C-0073.

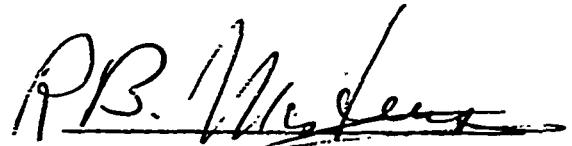
The author gratefully acknowledges the able assistance of R. G. Aurandt in carrying out the experiments. D. Nunberg did the photographic work.

This report, which documents research carried out from December 1970 through May 1972, was submitted for review and approval on 16 October 1972 to Lt Col E. W. Porter, DYA.

Approved

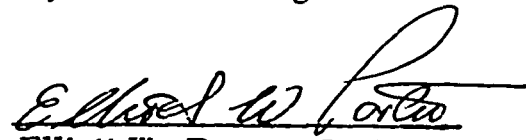


R. X. Meyer, Director
Plasma Research Laboratory
Laboratory Operations



R. B. Mortensen, Director
Hardened Reentry Systems
Ballistic Reentry Vehicles
Reentry Systems Division
Development Operations

Publication of this report does not constitute Air Force approval of the report's findings or conclusions. It is published only for the exchange and stimulation of ideas.



Elliott W. Porter, Lt Col, USAF
Asst Dir, Development Dir
Deputy for Technology

CONTENTS

FOREWORD	ii
ABSTRACT	iii
1. Introduction	1
2. Development of Induction Heating Apparatus for Thermal Stress Experiments	3
2.1 Basic Considerations	3
2.2 Shape of Specimen	5
2.3 Inductor Coil Design	8
2.4 Present Apparatus and Results	11
3. Conclusions and Recommendations	19
REFERENCES	21
APPENDIXES	
I. Matching of Graphite Load to Impedance of rf Oscillator	I-1
II. Calculation of Radial Temperature Distributions for Infinite Graphite Cylinder	II-1

FIGURES

1.	Calculated distributions of axial and azimuthal strains along inner surface of hollow ATJ-S graphite cylinder	4
2.	Shapes of graphite test specimens	6
3.	Magnetic flux concentrator	10
4.	Present arrangement of graphite thermal stress test apparatus	12
5.	Recordings of cooling water temperature in two heating tests leading to fracture	13
6.	Temperature correction for pyrometer readings taken through oil bath of apparatus in Figure 4	15
7.	Heating test in apparatus of Figure 4	16
8.	Fractured graphite specimens	17
I-1.	Schematic of rf oscillator load circuit	I-2
II-1.	Variations of thermal conductivity κ and electrical conductivity σ with temperature for ATJ graphite	II-2
II-2.	Heat conduction potential of ATJ graphite	II-3
II-3.	Radiation flux vs heat conduction potential of ATJ graphite	II-6
II-4.	Calculated temperature distributions in induction-heated ATJ graphite cylinder; low input	II-7
II-5.	Calculated temperature distributions in induction-heated ATJ graphite cylinder; high input, $f = 1.7$ MHz	II-8

1. Introduction

The tests described here were prompted by the continuing need in reentry vehicle design for quantitative information on the thermal fracture of graphite.* It was important to determine whether the severe conditions leading to thermal fracture could be produced in an inexpensive laboratory experiment or whether one would have to expand the more expensive thermostructural rocket test program to satisfy the needs of the designer. One possibility for a laboratory experiment was induction-heating of graphite with the large rf plasma generator of The Aerospace Corporation. Therefore, this facility was modified for the purpose, and temperature gradients were produced in hollow graphite cylinders by induction heating of the outer surface and water-cooling of the inner surface. The two major problems encountered in this experiment were electric breakdown caused by the nearness of the inductor coil to a hot surface and leakage at the junctions of the expanding graphite and the coolant tubing. These and other problems were gradually overcome in one year's time through numerous changes to the apparatus. In the present arrangement, temperature gradients in excess of $1000^{\circ}\text{K}/\text{cm}$ can be obtained; these have proved to be sufficient to break ATJ-S graphite. No systematic effort was made to obtain the complete information needed for establishing a fracture criterion, as this will be the objective of the next phase. In this report, the development of the apparatus and its final arrangement are described in sufficient detail for others to do the testing. The important considerations for matching the specimen load to the rf heater impedance are contained in Appendix I.

Because it is very difficult to measure the radial temperature distribution in the specimen without affecting fracture resistance and heating pattern, a simple calculation method is derived in Appendix II that is based on an analytical solution of the energy balance equation for an infinite cylinder. The solution takes into account the frequency dependence of the heat source distribution, the

*A recent survey of unclassified information on graphite nosetips was made by P. J. Schneider, et al. [1].

temperature dependence of the thermal conductivity, and the radiation losses. With reliable data on material properties, the method should provide more accurate results than can be expected from measurements.

2. Development of Induction Heating Apparatus for Thermal Stress Experiments

2.1. Basic Considerations

Some estimate of the power required to break a specimen of ATJ-S graphite by thermal stresses can be obtained from calculations reported by W. R. Grabowsky.* Figure 1, reproduced from these calculations, shows the distributions of longitudinal and azimuthal strains along the inner surface of a hollow cylinder whose dimensions are given in the top portion of the figure. With temperatures of $\sim 2600^\circ\text{K}$ and 500°K at the outer and inner surfaces, respectively, it is expected that the strains, especially axial, will exceed the breaking limit. The average temperature gradient for this case is $2100^\circ\text{K}/1.54\text{ cm}$ or $1360^\circ\text{K}/\text{cm}$; the average thermal conductivity, obtained from Fig. II-1, is $\sim 0.1\text{ cal/sec cm}^\circ\text{K}$ or $\sim 0.4\text{ W/cm}^\circ\text{K}$. Thus, the heat flux per cm^2 area is $\sim 550\text{ W/cm}^2$ or, for the total area of $\sim 100\text{ cm}^2$, 55 kW. With the addition of 10% for radiation and convection losses, the total power requirement is 60 kW. Although this value is within the capability of the Aerospace rf heater, it requires careful matching and efficient coupling to the load. Efficient coupling is obtained if the induction coil is close to the specimen, but as this interferes with protecting the coil from the heat, a compromise must be made.

Another compromise is necessary with respect to the operating frequency. At the conductivity of graphite, $\sigma \approx 1000$ to 1500 mho/cm , a frequency of 10^4 to 10^5 Hz , skin depth $\sim 1\text{ cm}$, would be desirable for efficient volume heating. But this would require major changes in the circuitry of the oscillator that previously has operated in the MHz range. In the calculations of Appendix I, therefore, $f = 1\text{ MHz}$ has been assumed. Actual tests were run at $f \approx 1.4$ to 1.7 MHz .

*W. R. Grabowsky (The Aerospace Corporation, SBO) Memorandum to The Aerospace Corporation, GO, Subject: Graphite Thermal Stress Experiment (23 January 1969).

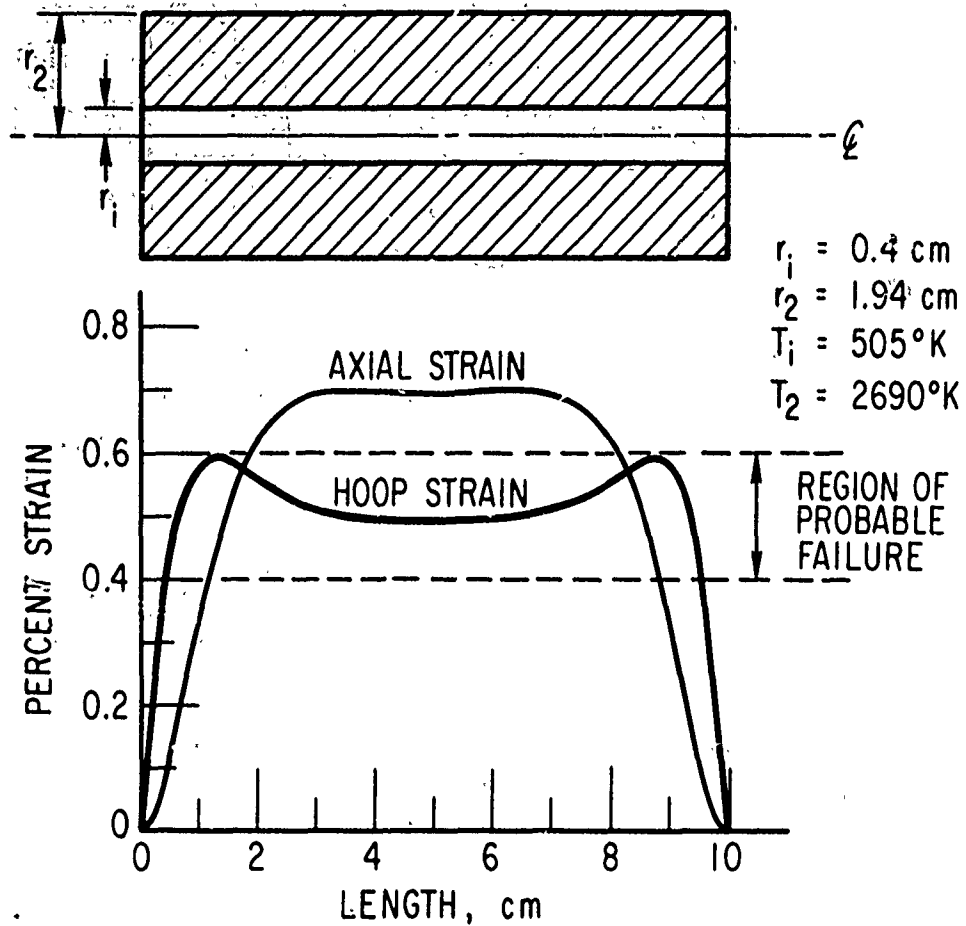


Figure 1. Calculated distributions of axial and azimuthal strains along inner surface of hollow ATJ-S graphite cylinder

2.2. Shape of Specimen

All specimens tested were hollow ATJ-S graphite cylinders with an o.d. of 3.8 cm and a length of 10 cm. These dimensions turned out to be nearly optimal for the production of fracture, with the available laboratory facilities, in a heating zone that was nearly uniform axially. For an appreciably longer cylinder, the generator power would have been insufficient and problems also might have arisen in the coolant flow because of the larger resistance and the higher exit temperature (boiling). For a cylinder with an appreciably lower l/d ratio, it would have been difficult to obtain a sufficiently uniform axial temperature in the midzone where fracture was likely to occur. Changes were made only in the diameter of the bore and in the method of connection with the coolant flow tubing. The first configuration is shown in Fig. 2a. Except for the conical sink at the front surface, this shape is the same as that used in earlier experiments at the Aerodynamics and Propulsion Research Laboratory. The use of a threaded neck and Swadgelok fitting to connect the specimen to copper tubing of slightly smaller diameter than that of the bore ensures freedom from mechanical stresses. The gap between tubing and cylinder is filled with a gallium-indium alloy, which consists of 76% Ga and 24% In, that is liquid at room temperature and provides thermal contact. Although the boiling point of this alloy is above 2000°K, it was useful only as long as the heating rates were below ~ 1.5 kW/cm. At higher rates, it was partly driven out of the gap, probably by gas liberated in the hot graphite, and seemed to make only spot contact. This was indicated by the low temperature gradients inferred from pyrometer readings at the front surface that were found to be $\sim 200^\circ\text{K}/\text{cm}$ and corresponded to radial heat fluxes of only 0.7 kW/cm. Therefore, most of the heat input must have been conducted in the axial direction toward the neck.

In order to avoid these problems, the neck, inner tubing, and liquid metal were eliminated, and the cooling water was led directly into the bore after the graphite pores had been sealed with an electrolytically deposited copper coating that was 0.05 to 0.1 mm thick. Also, the bore was widened from 8 to 13 mm diameter for the following reasons: First, calculations described in Appendix II

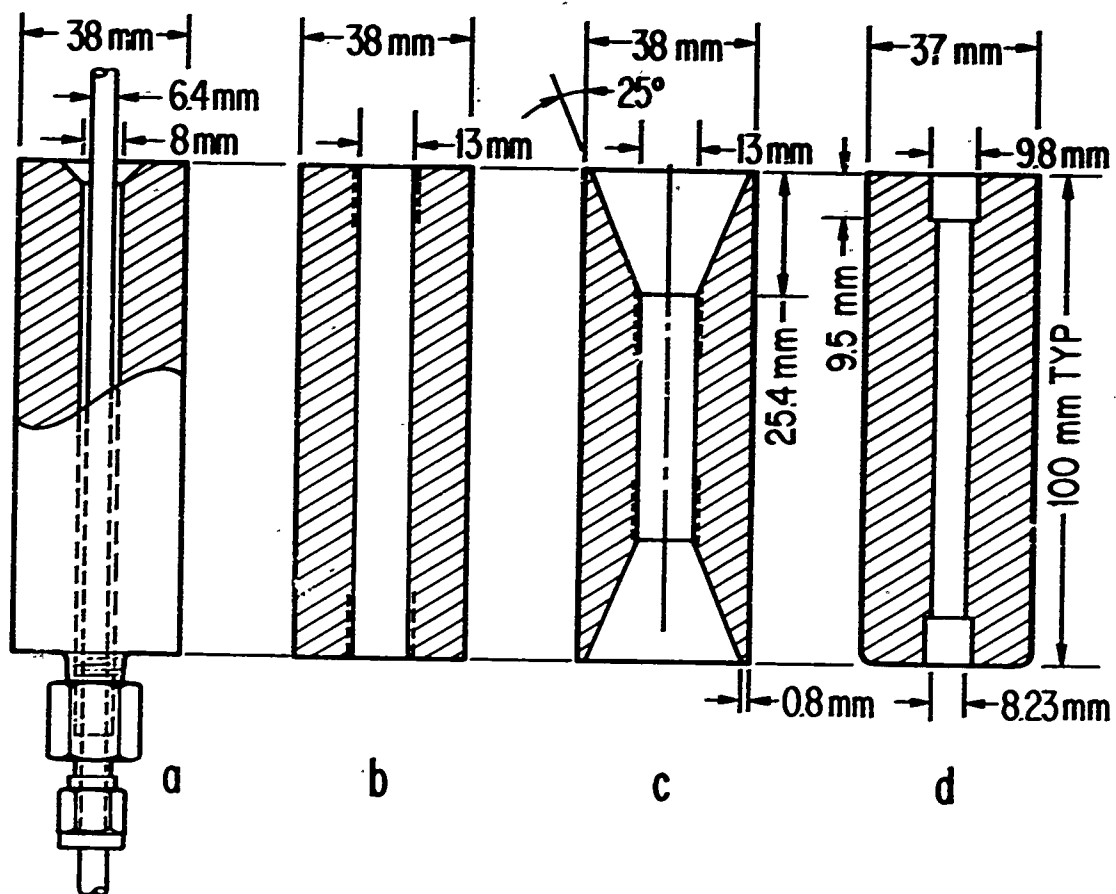


Figure 2. Shapes of graphite test specimens

had indicated that, at a desired input of 4 kW/cm, the temperature at the outer surface would exceed the apparatus safety limit of $\sim 2000^{\circ}\text{K}$ (Fig. II-5). Second, the wider cross section allowed the cooling flow rate to be raised from ~ 2.5 to 4 gpm, which eliminated shaking of the specimen caused by nucleate boiling. Copper tubing ends, with the same i.d., were threaded 0.5 in. deep into the graphite and sealed with Viton O-rings (Fig. 2b). Because the O-rings burned up on the graphite side during heating, they were replaced by V-profile copper rings, which were compressed for proper sealing. This introduced mechanical stresses into the specimen that were not considered admissible; therefore, the gaskets were eliminated, and the tubing was soft-soldered to the copper coating.

When the solder melted during testing, silver soldering was considered, which requires silver coating of the graphite interior. This approach was abandoned because the silver adhered to the graphite only after the binding material of the graphite had been driven out by heating the sample in a furnace. Finally, lead was used because it has a sufficiently high melting point, and could be soldered onto the copper.

The specimens were then prepared by the following procedure: Lead was filed into fine particles that were mixed with conventional paste soldering flux (Douton Co.'s NOKORODE). This mixture was then painted onto both mating surfaces, which had been prewarmed to assist in the flowing of the flux and solder. These surfaces were then heated separately to a temperature at which the lead filings would melt and wet the associated surfaces. Excess solder was wiped from the tube and shaken from the sample. The now lightly leaded surfaces were allowed to cool to a point where they were still warm, given a light coating of the flux and solder mixture, and then put together in their finished positions. When the fit was loose, a sufficient amount of the lead filings was placed around the tubing, at the point where it entered the sample, to fill the annulus. The entire assembly was then heated to the melting point of lead and allowed to cool slowly. The bore of the sample and associated end fittings were then given a coating of conventional lead and tin solder (Johnson's FLUX-'N-Solder) paste and again heated to the appropriate temperature to seal

any porosity in the copper plating. The lead and tin solder is adequate in this application, as it is in direct contact with the water flow.

Because the desired power inputs, up to 5 kW/cm (Fig. II-5), could not be generated over the full length of the sample, an attempt was made to produce such inputs locally by tapering the ends (Fig. 2c). Here heating occurred over the full length, whereas cooling was limited to one-half of the specimen length so that an axial convergence of the heat flux in the ratio 2:1 occurred. However, fracture could not be achieved with this shape, as the total power input had to be limited to ~20 kW because of the increased surface temperature. Also, it would be more difficult to determine the magnitude of the thermal stress from the two-dimensional heat flux pattern in this geometry.

In the subsequent version (Fig. 2d), axial convergence was abandoned in favor of increased radial convergence that resulted from reducing the bore diameter again to 8 mm. The coolant flow rate was maintained and eventually even increased to 5 gpm by putting a booster pump into the city water line. Also, it was possible to eliminate the threading and still retain sufficient rigidity. Finally, the sharp edge at the lower end, adjacent to the side of the inductor carrying the high rf potential, was rounded off to reduce the formation of corona discharges. This specimen shape, which is also shown in the final arrangement in Fig. 4, was used in later tests where fracture occurred.

2.3. Inductor Coil Design

From the considerations in Appendix I, it follows that the inductor coil should have at least 16 turns over a length of 10 cm. In order to produce this turn density, hollow-core, rectangular copper tubing, with a cross section of $3.2 \times 6.4 \text{ mm}^2$, was wound over the small side into a 17-turn coil that had a 2.6-cm inner radius. The coil was then silver-plated and connected to the terminals of the plate tank circuit, which also provided waterflow for cooling. In the first heating tests, the coil was operated in air and separated from the graphite specimen by a clear quartz tube. When the rf voltage on the coil had reached ~6 kV and the graphite surface became red hot, corona filaments formed on the graphite surface next to the end of the coil carrying the high

potential. These filaments gradually grew into arcs, softened the quartz, and finally pierced it. At other times flashovers occurred between the coil turns, which caused irreparable leaks.

In order to avoid these problems, an alternative configuration was tested that dates back to an idea of Babat and Losinsky [2]; it is termed a magnetic flux concentrator. A photograph of the device is shown in Fig. 3; the dimensions in inches can be inferred from the size of the 6-in. scale in the picture. The device consists of two coaxial, slotted, copper cylinders that are silver-plated and are connected at the slots by trapezoidal copper plates. The length of the interior cylinder, at 5 in., is only one-third that of the outer; thus, the linear density of a current induced in the latter is increased by a factor of 3. The tightly fitting inductor coil has 20 turns of square copper tubing and is insulated by a pyrex tube from the concentrator that is at floating potential. The graphite specimen fits closely into the inner cylinder and is not near a high rf potential. The danger of arcing between coil turns is also greatly reduced by the wide turn spacing. The entire length of the specimen can be observed through the slot.

In tests with this configuration, the plate voltage of the generator could be run up to its maximum value of 10 kV without a breakdown. But the power input to the graphite at this voltage, and at a frequency $f \sim 2$ MHz, was only 15 kW, which is not higher than could be obtained with the small inductor coil at ~ 7 kV. Probably, the poor efficiency resulted from poor coupling, which was caused by the large difference in coil and load diameters, and from ohmic losses in the concentrator. Tapping the inductor coil, which lowered the impedance of the system, brought little improvement in efficiency. Although some improvement could have been obtained by optimizing the design, it was still questionable whether the needed power input could ever be reached. Therefore, efforts were focused on overcoming the problems associated with direct heating, and further work with the flux concentrator was abandoned.

Reproduced from
best available copy.

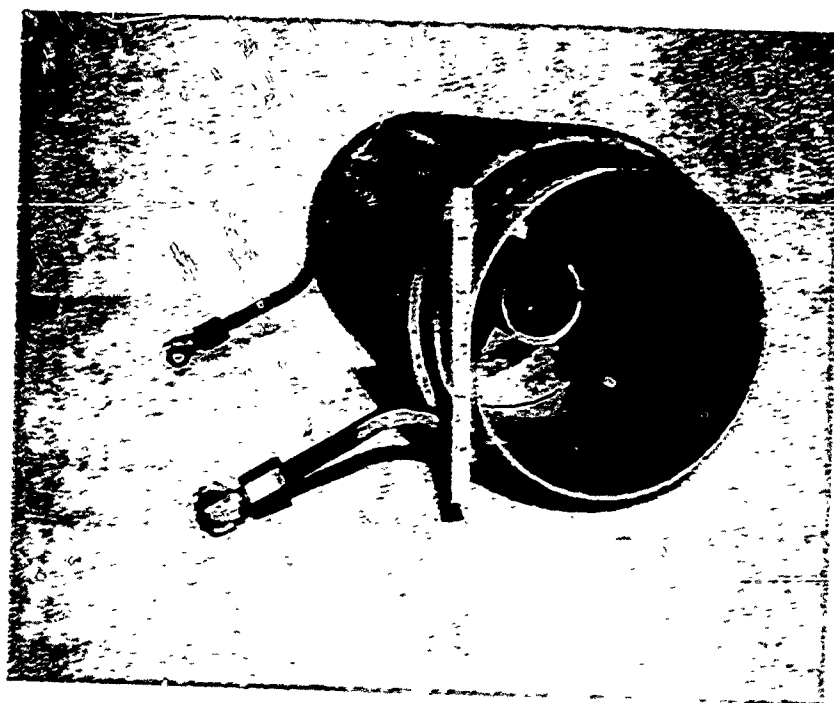


Figure 3. Magnetic flux concentrator

2.4. Present Apparatus and Results

In the final apparatus, the original inductor coil was used again, but it was placed in a bath of circulating oil (Fig. 4). The purpose of the oil was to provide insulation and additional cooling. The first tests were made with Shell Diala Oil AX, which smoked heavily when the graphite became red hot and produced a fire hazard. Noncombustible Monsanto Ascaral, the second candidate, apparently has poor insulating qualities, because it permitted small sparks to form at the high voltage end of the coil and it decomposed into black filaments, possibly carbon, which after a short time produced breakdown between turns of the coil. The final choice was Kinney vacuum oil Kinelube 220, which is highly viscous at room temperature, but has a flash point of 500°F and generally proved satisfactory after outgassing. The GE perfluorinated oils were considered, but were not used because, although they may be ideal for this purpose, the cost is prohibitive.

As shown in Fig. 4 there is, in addition to the vycor tube of the oil vessel, a quartz tube separating the coil from the graphite sample. For cooling, nitrogen gas was blown, at 30 psi, through the narrow annular gap between the tubes. A radiation shield, which consisted of a slotted tantalum cylinder, was inserted into the gap, but proved to be useless. The metal was apparently heated by capacitive currents and gradually burned up. The quartz tube can be replaced by a specially fabricated thin-walled Mullite tube (Coors, Golden, Colo.) that can stand temperatures about 400°C higher, but for ATJ-S graphite this has not been necessary.

The flow rate of the cooling water through the sample is metered, and the difference between inlet and outlet temperatures is registered, through a thermistor bridge, on an X-Y recorder. Examples of two tracings are shown in Fig. 5. Power input is raised gradually over periods of 4 to 5 min by increasing the plate voltage from 3 kV (onset of oscillations) to ~8.5 kV, with minor retuning in between. This increase in plate voltage is shown to correspond to an increase in water temperature of 28°C. At a flow rate of 5 gpm, this temperature rise corresponds to a heat flux through the sample of 38 kW. At this point, fracture occurs and the generator is turned off automatically by

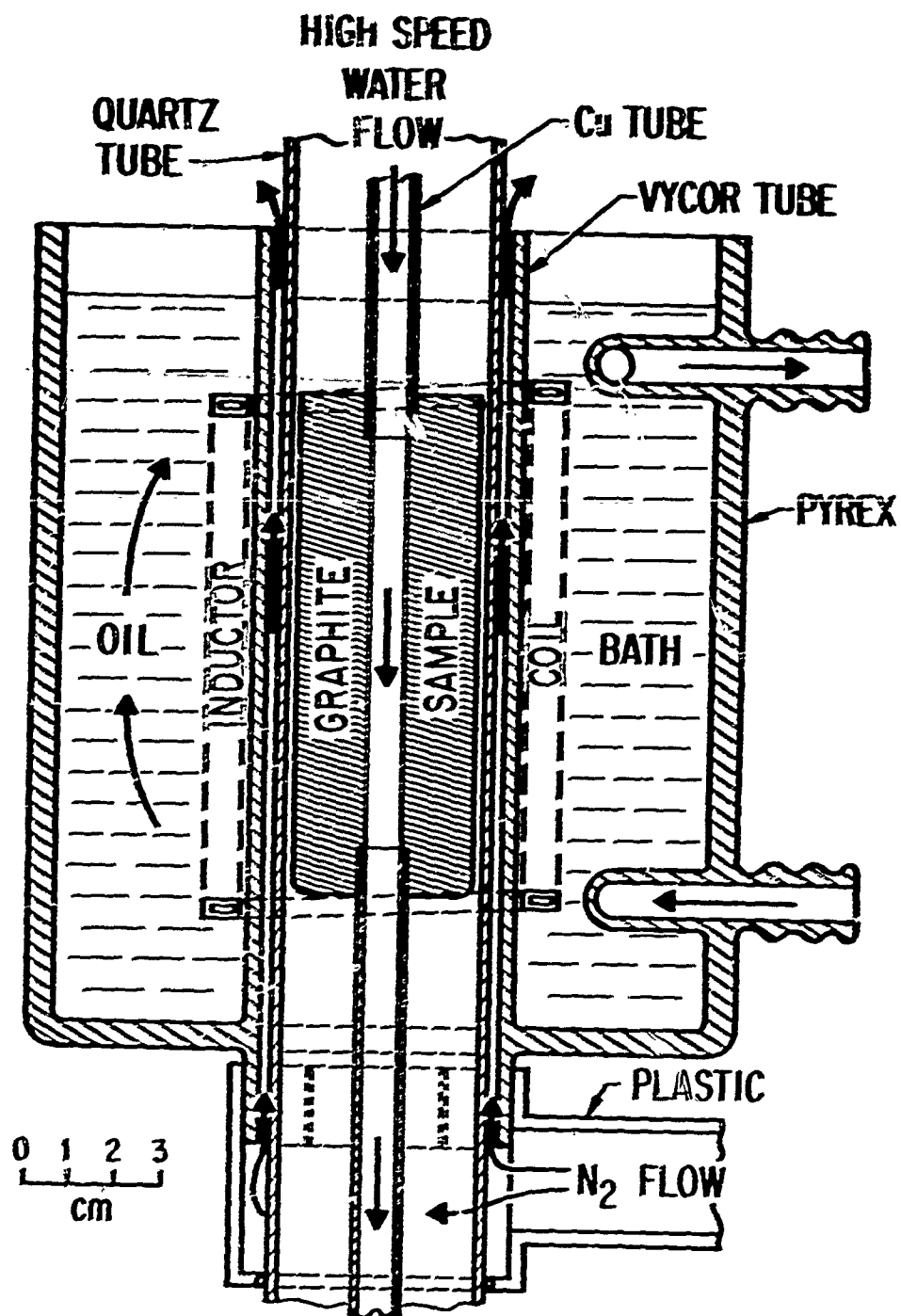


Figure 4. Present arrangement of graphite thermal stress test apparatus

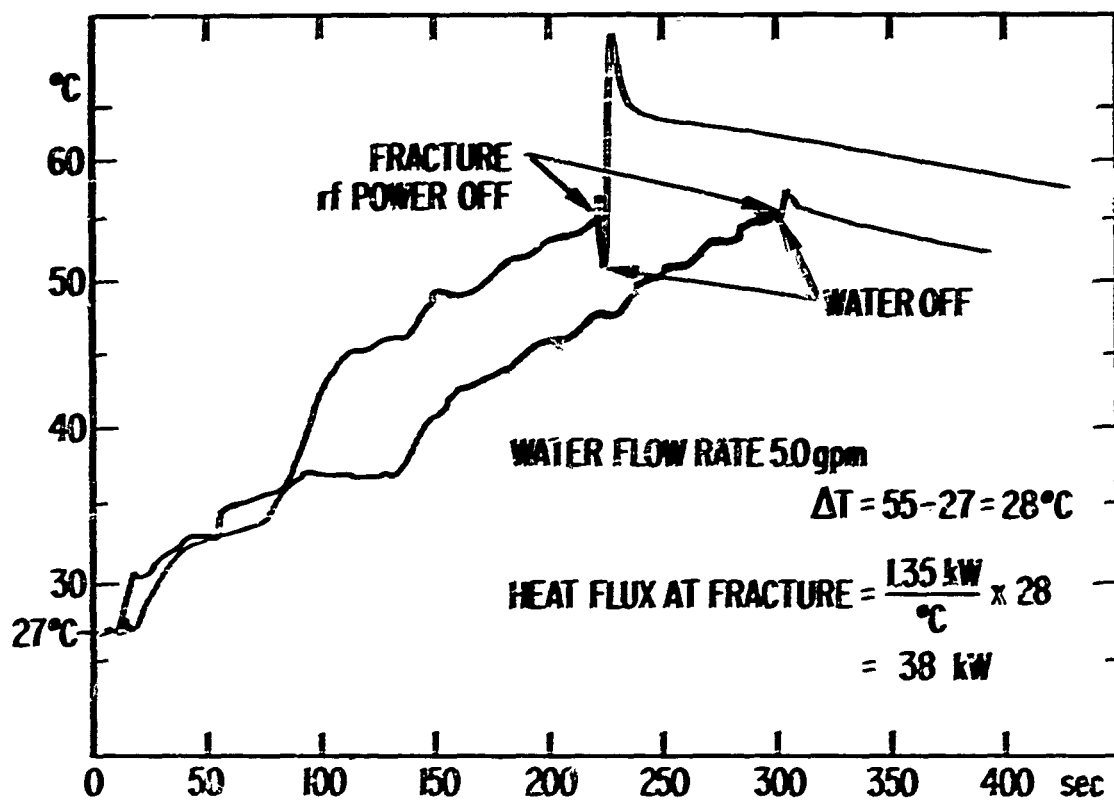


Figure 5. Recordings of cooling water temperature in two heating tests leading to fracture

the sudden change in load so that the coolant temperature drops instantaneously. Also, depending on the manner of fracturing, a certain amount of spillage takes place and the flow is shut off manually within seconds. The temperature rises again temporarily. At a flow rate of 5 gpm, water pressures upstream and downstream of the specimen are ~28 and 7 psi, respectively. These pressures are negligible compared with the thousands of psi induced thermally.

The surface temperature of the specimen is measured with an optical pyrometer ("Pyro" Bergenfield, N. J.) either at the upper front surface with the aid of a 45-deg mirror or on the side between the turn spacings. In the latter case, a small correction must be applied because of optical absorption by the oil. This correction has been obtained from the curve in Fig. 6. Side-on and end-on photographs of apparatus and samples taken during a heating test are shown in Figs. 7a and 7b. The brightness distribution of the specimen in Fig. 7a indicates that the longitudinal distribution of the surface temperature is not uniform, but has a maximum near the midsection. Its value at the moment of fracture has been measured, in two cases, to be between 1900° and 2000° K. Assuming the temperature at the inner surface to equal the water boiling temperature, we obtain a temperature difference between the surfaces of 1600° K or an average gradient of 1050° K/cm. The diameter of the sample in Fig. 7b has been compared with that before heating and was found to have expanded by 1.5%.

All twelve samples that were fractured with the apparatus were leak-tested and carefully inspected for cracks before installation. Photographs of four samples are shown in Fig. 8. The sample in Fig. 8b, which has several lengthwise hairline cracks, is representative of several that were heated faster (total heating time ~2 min) than the others. The fast-heated samples seem to break at ~10% lower power and usually stay in one piece; whereas, the samples heated normally over 4 to 5 min break into two or three pieces, as seen in Figs. 8a, c, and d.

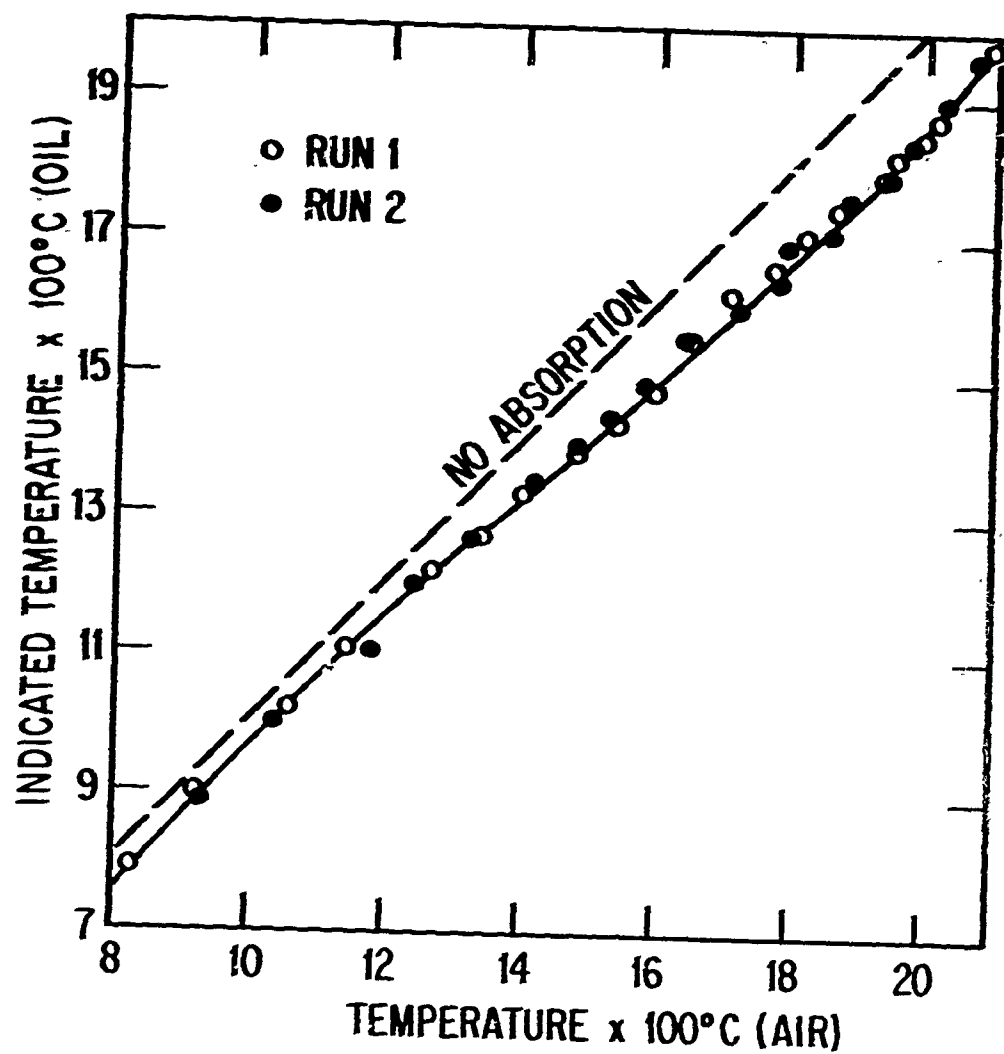
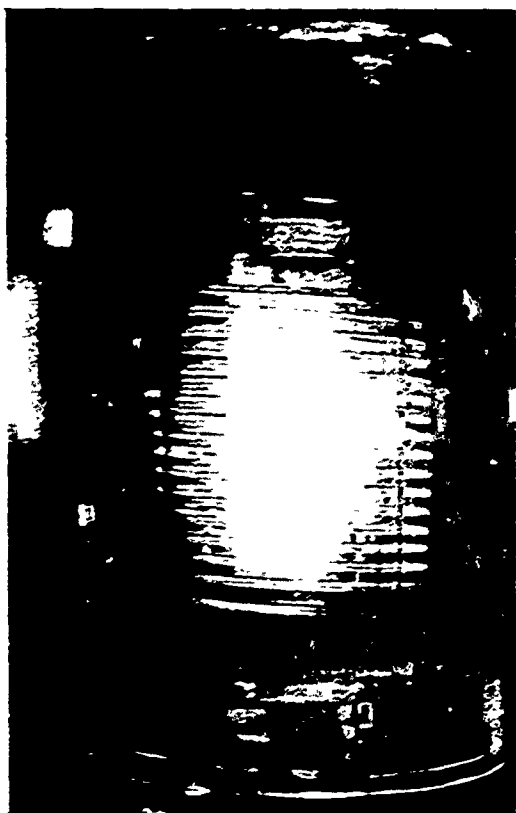
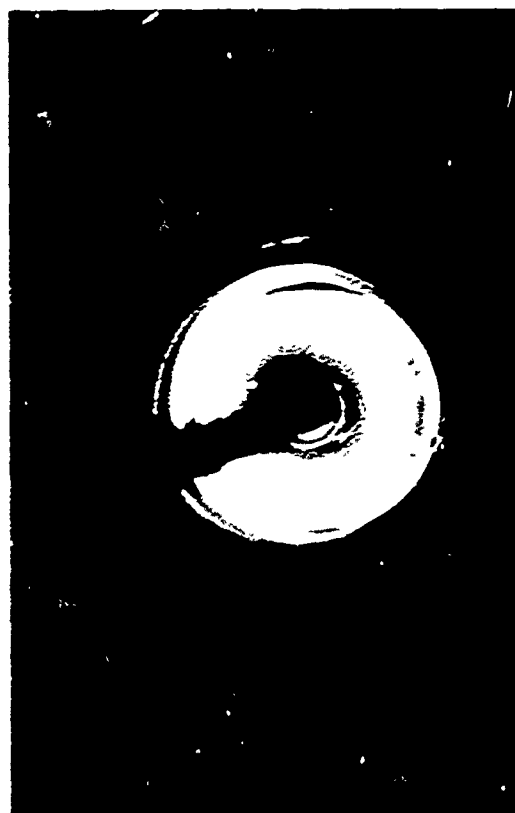


Figure 6. Temperature correction for pyrometer readings taken through oil bath of apparatus in Fig. 4.
Oil: Kinlube 220 of Kinney Vacuum Equipment Co.



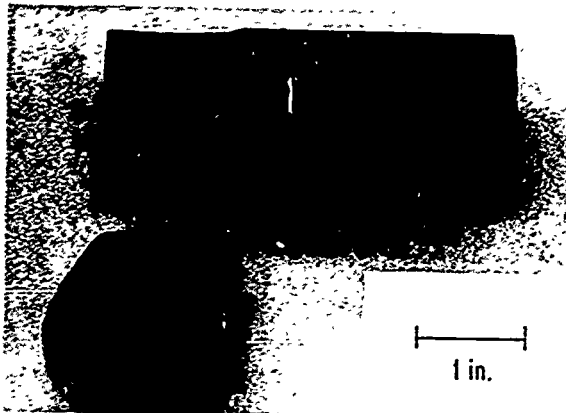
(a) SIDE-ON VIEW



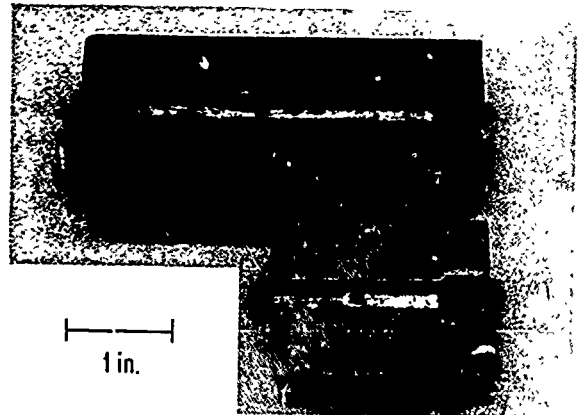
(b) END-ON VIEW OF SAMPLE

Figure 7. Heating test in apparatus of Fig. 4

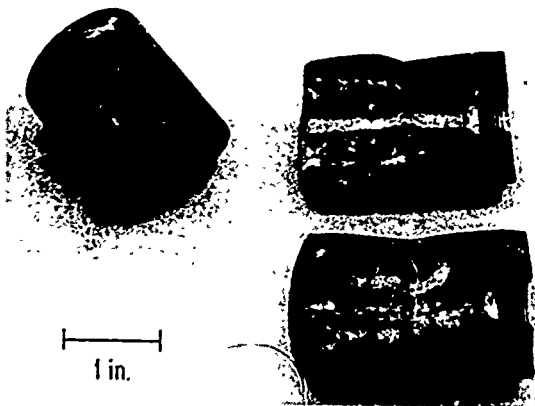
Reproduced from
best available copy.



(a) 72 MAR 17



(b) 72 APR 28



(c) 72 MAY 5



(d) 72 MAY 11

Figure 8. Fractured graphite specimens

3. Conclusions and Recommendations

The results of this first exploratory phase have demonstrated that the apparatus and technique developed at the Plasma Research Laboratory can produce thermal failure in ATJ-S graphite cylinders. Since the load-matching procedure was not carried to the optimum and the full plate voltage was not required for fracture, there is still a considerable power reserve in the system, which might be used either to break stronger types of graphite or to improve conditions for difficult measurements.

Although the data obtained in this phase are neither complete nor systematic, they already permit some tentative conclusions. First, there is no striking disagreement with the theoretical predictions reported by W. R. Grabowsky. Whereas the temperature gradients measured are $\sim 25\%$ lower than those calculated in the example in Fig. 1, the failure limit is exceeded by the axial strain in that example by $\sim 30\%$. Therefore, there is no need at this time to revise design specifications based on that theory.

Second, the rate of rise in power input appears to affect fractural behavior, which means that the fracture criterion depends on the flight trajectory; therefore, a closer investigation of this phenomenon is recommended. With the present self-excited oscillator, full power output could not be reached before 90 sec because the plate voltage must be raised gradually; however, faster rises could be obtained by operating the installation as a power amplifier with an available 5-kW Lepel induction heater as the modulator. This would allow continuous application of full plate voltage, with the output determined by the degree of modulation. It is expected that the transition from zero to full output could then be accomplished in 1 sec or less.

In order to obtain a more nearly uniform temperature distribution over the length of the sample, an inductor coil with higher turn density at the ends is recommended to compensate for end losses by increased heating. Although, for a fixed turn spacing, the distribution can be strictly uniform for one temperature only, the coil would reduce considerably the two-dimensionality of the temperature field so that simple one-dimensional calculations,

similar to those in Appendix II, could be applied with confidence. Also, it would give more significance to the total heat flux measurements that, at present, are averages of an unknown distribution.

Finally, in order to check more directly the theoretical predictions as exemplified in Fig. 1, it would be desirable to measure the axial and radial strains of the inner surface at the moment of failure. For the specimens tested, the absolute axial dilatation would be ~ 0.5 mm. It could be measured accurately with an optical interference system that is attached to the coolant tube stubs and combined with a fringe (pulse) counting recorder.

Measurement of the radial dilatation at the inner radius is more difficult because it is smaller and interfered with by the coolant. It may be possible to make the measurement by means of the photographic technique used to measure the dilatation at the outer radius (Fig. 7b). If the facility is operated as a power amplifier, as mentioned before, it may be possible to cause fracture by shock heating and eliminate the need for water-cooling. In this case the bore of the cylinder would become accessible to direct strain measurements. The feasibility of this idea can be determined only by experiments.

REFERENCES

1. P. J. Schneider, et al., "Design of Graphite Nosetips for Ballistic Reentry", Paper No. 72-705 presented AIAA 5th Fluid and Plasma Dynamics Conference, Boston, 26-28 June 1972.
2. G. Babat and M. Losinsky, "Concentrator of Eddy Currents for Zonal Heating of Steel Parts," J. Appl. Phys. 11, 816-23 (1940).
3. E. May, Industrial High Frequency Electric Power, Chapman and Hall Ltd., London (1949).
4. Y. S. Touloukian, ed., Thermophysical Properties of High Temperature Materials, Vol. I, The MacMillan Co., New York (1967).
5. H. U. Eckert, "Analysis of Thermal Induction Plasmas Dominated by Radial Conduction Losses," J. Appl. Phys. 41, 1520-28, (1970).

APPENDIX I

Matching of Graphite Load to Impedance of rf Oscillator

The rf heater of The Aerospace Corporation is a tuned-plate, tuned-grid, self-excited oscillator operating in or near the class B mode with four GE 890 triodes in parallel. Each tube is rated for a plate current of 5 A. At this current and at the maximum available plate voltage of 10 kV, an internal resistance of $\sim 800 \Omega$ per tube is obtained from the tube chart. The internal resistance of the heater is therefore

$$R_i \approx 200 \Omega \quad (1)$$

For maximum power transfer, R_i must be matched by the external resistance R_e . Since R_e results from a complex arrangement and can be determined only approximately and since a mismatch is much less critical if $R_e > R_i$, we aim for

$$R_e \approx 400 \Omega \quad (2)$$

As indicated schematically in Fig. I-1, R_e is formed by the resonating plate tank circuit $C R_1 L_1$ and the secondary or load circuit $L_2 R_2$ if the small impedance of the blocking capacitor C_B is disregarded. The two circuits are coupled through the mutual inductance M . The value of R_e is given by

$$R_e = \frac{L_{\text{eff}}}{C R_{\text{eff}}} \quad (3)$$

where L_{eff} and R_{eff} are the effective inductance and resistance, respectively, as seen by the resonating circuit. Their values are determined by the relationships [3]

$$L_{\text{eff}} = L_1 - \frac{(\omega M)^2 L_2^2}{R_2^2 + (\omega L_2)^2} \quad (4)$$

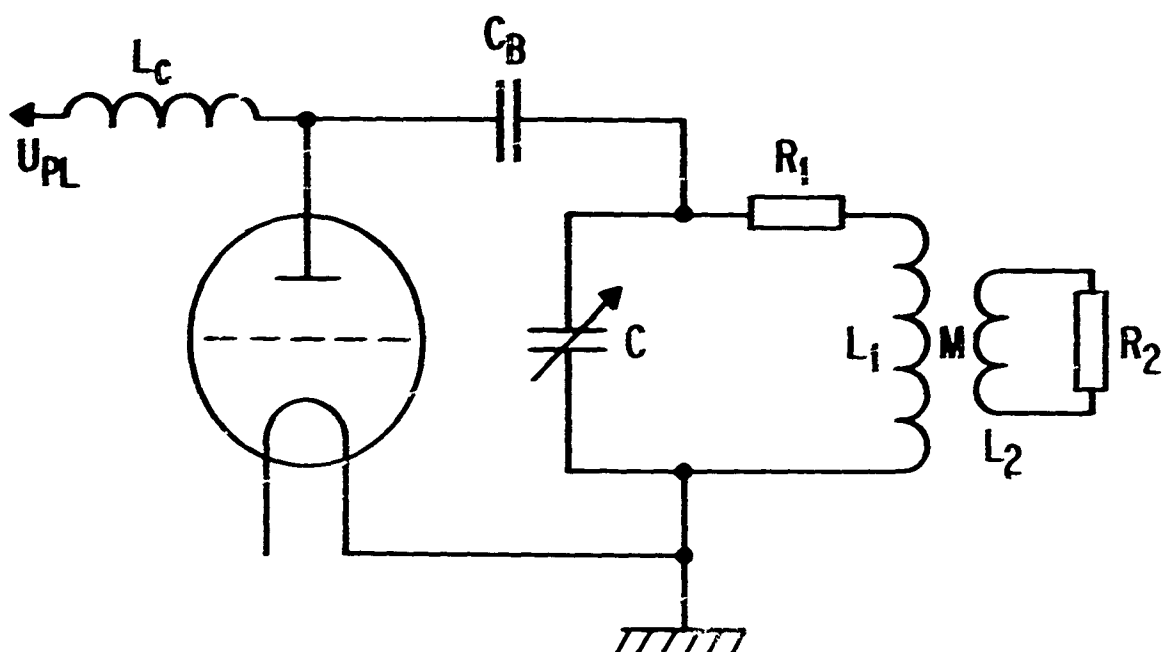


Figure I-1. Schematic of rf oscillator load circuit.
Only one of four tubes is shown

$$R_{\text{eff}} = R_1 + \frac{(\omega M)^2 R_2^2}{R_2^2 + (\omega L_2)^2} \quad (5)$$

where $\omega = 2\pi f$. The practical lower limit on the generator frequency is believed to be about

$$f = 1 \text{ MHz} \quad (6)$$

Disregarding the effect of R_{eff} on frequency, we use the relationship

$$f \approx \frac{1}{2\pi(L_{\text{eff}} C)^{1/2}} \quad (7)$$

The quality factor Q of the circuit is taken as

$$Q = \frac{\omega L_{\text{eff}}}{R_{\text{eff}}} = 10 \quad (8)$$

From (6), (7), and (8), we obtain

$$\frac{L_{\text{eff}}}{R_{\text{eff}}} = 1.6 \times 10^{-6} \quad (9)$$

With (2) and (3), we then obtain for the tank capacitance

$$C = 4000 \text{ pF} \quad (10)$$

and further

$$L_{\text{eff}} = 6 \mu\text{H} \quad (11)$$

and

$$R_{\text{eff}} = 3.8 \Omega \quad (12)$$

The circulating current in the tank circuit is limited by the permissible rf peak voltage \hat{U}_1 , which should stay $\sim 10\%$ below the plate voltage U_p .

With $U_{p \text{ max}} = 10 \text{ kV}$, we have $\hat{U}_1 \approx 9 \text{ kV}$ and the maximum power dissipation, which includes circuit losses, is

$$P_{\text{max}} = \frac{\hat{U}_1^2}{2 R_e} \approx 100 \text{ kW} \quad (13)$$

This value is considerably above the 60 kW estimated for the specimen in Section 2.1.

The rms circulating current is

$$I_1 = \frac{\hat{U}_1}{\sqrt{2} \left[(\omega L_{\text{eff}})^2 + R_{\text{eff}}^2 \right]^{1/2}} \approx \frac{\hat{U}_1}{\sqrt{2} \omega L_{\text{eff}}} \approx 170 \text{ A} \quad (14)$$

The distribution of the secondary current I_2 in the graphite specimen, which has the dimensions $r_2 = 1.9 \text{ cm}$ and $l_2 = 10 \text{ cm}$, is characterized by the skin depth

$$\delta = \left(\frac{2}{\sigma \mu \omega} \right)^{1/2} \quad (15)$$

With $\mu = \mu_0 = 1.256 \times 10^{-8} \frac{\text{Vsec}}{\text{A cm}}$, $\sigma \approx 1000 \frac{\text{A}}{\text{Vcm}}$ *, and $\omega = 6.28 \times 10^6 \text{ sec}^{-1}$, the values

$$\delta \approx 0.16 \text{ cm} \quad (16)$$

and

$$\frac{r_2}{\delta} \approx 12 \quad (17)$$

are obtained. The resistance R_2 seen by the voltage U_2 induced around the periphery is

$$R_2 = \frac{U_2}{I_2} = \frac{2\pi r_2 E_2}{l_2 \int_0^{r_2} E dr} \quad (18)$$

For $\frac{r_2}{\delta} > 10$, the variation of the induced electric field E with r is closely approximated by the power law

$$E = E_2 \left(\frac{r}{r_2} \right)^{\frac{r_2}{\delta}} \quad (19)$$

* The data in Fig. II-1 indicate that a more appropriate mean value for σ would be 1400 mho/cm. These data were obtained after the calculations in this appendix had been made. Because of their exploratory nature and as σ enters only with the square root, a revision was not considered worthwhile.

so that

$$\int_0^{r_2} E dr = \frac{r_2 E_2}{r_2/\delta + 1} \quad (20)$$

and

$$R_2 = \frac{2\pi \left(\frac{r_2}{\delta} + 1\right)}{l_2 \sigma} \approx 2.2 \times 10^{-3} \Omega \quad (21)$$

To dissipate 60 kW at this value of R_2 requires a secondary current

$$I_2 = \left(\frac{P}{R_2}\right)^{1/2} = 2700 \text{ A} \quad (22)$$

Since $\frac{R}{\delta} \gg 1$ we can set

$$\frac{I_2}{I_1} \approx \frac{N_1}{N_2} \quad (23)$$

where N is the number of turns over the length of the work piece. With $N_2 = 1$ and $I_2 = 170 \text{ A}$, disregarding end effects, we obtain for the number of turns of the inductor coil

$$N_1 = \frac{2700}{170} \approx 16 \text{ turns} \quad (24)$$

The value of L_2 follows from the formula for a coil of finite length [3]

$$L_2 = 1.36 \times 10^{-2} \mu\text{H} \quad (25)$$

Therefore, $\omega L_2 = 8.5 \times 10^{-2} \approx 10 R_2$, and it is permissible to disregard R_2^2 in comparison with $(\omega L_2)^2$ in Eqs. (4) and (5). M and L_2 are related through

$$MI_1 = L_2 I_2 \quad (26)$$

With Eq. (23) and $N_2 = 1$, Eq. (26) yields

$$M = N_1 L_2 \quad (27)$$

and Eqs. (4) and (5) reduce to

$$L_1 = L_{\text{eff}} + N_1^2 L_2 \quad (28)$$

$$R_1 = R_{\text{eff}} - N_1^2 R_2 \quad (29)$$

Numerical values yield

$$L_1 = 6 \pm 3.5 = 9.5 \text{ } \mu\text{H and}$$

$$R_1 = 3.8 - 2.1 = 1.7 \Omega$$

It remains to determine the physical dimensions of L_1 . If we take

$l_1 = l_2 = l = 10 \text{ cm}$, only the radius r_1 remains free. From the short coil formula [3]

$$r_1 = 2.7 \text{ cm}$$

is obtained for the above values of L_1 , N_1 and l . These data for the inductor coil have been used in the tests, but the frequency was lowered only to 1.4 MHz when it was found that fracture could be produced at this frequency with total power dissipation in the tank circuit ~50 kW.

APPENDIX II

Calculation of Radial Temperature Distributions for Infinite Graphite Cylinder

In steady state, the specimen loses the heat generated by ohmic dissipation mostly by conduction and surface radiation. Convection losses are held low and may be disregarded. Radiation is accounted for in the boundary condition for the outer surface. The energy balance equation consists, therefore, of only the following two terms

$$\frac{1}{r} \frac{d}{dr} (rk \frac{dT}{dr}) + \sigma E^2 = 0 \quad (30)$$

The variations of thermal conductivity k and electrical conductivity σ with temperature for ATJ^{*} graphite are shown in Fig. II-1 [4]. Whereas for σ a mean value, $\bar{\sigma}$ may be used without severely affecting the results, this does not seem permissible for k . To linearize the equation, it is therefore advantageous to introduce the heat conduction potential S as is common with gaseous plasmas [5]. S is defined by

$$S = \int_0^T k dT \quad (31)$$

The evaluation of Eq. (31) is shown in Fig. II-2. For the variation of E with r , we use Eq. (19). Setting $r/r_2 \equiv x$, we can write Eq. (30) in the form

$$\frac{1}{x} \frac{d}{dx} (x \frac{dS}{dx}) + r_2^2 \bar{\sigma} E_2^2 x^{2q} = 0 \quad (32)$$

where $q \approx r_2/\delta$ for $r_2/\delta > 2$ [4]. The first integration of Eq. (32) yields

$$x \frac{dS}{dx} + \frac{r_2^2 \bar{\sigma} E_2^2}{2q+2} x^{2q+2} = C \quad (33)$$

*Property data for ATJ-S graphite were not available at the time these calculations were made.

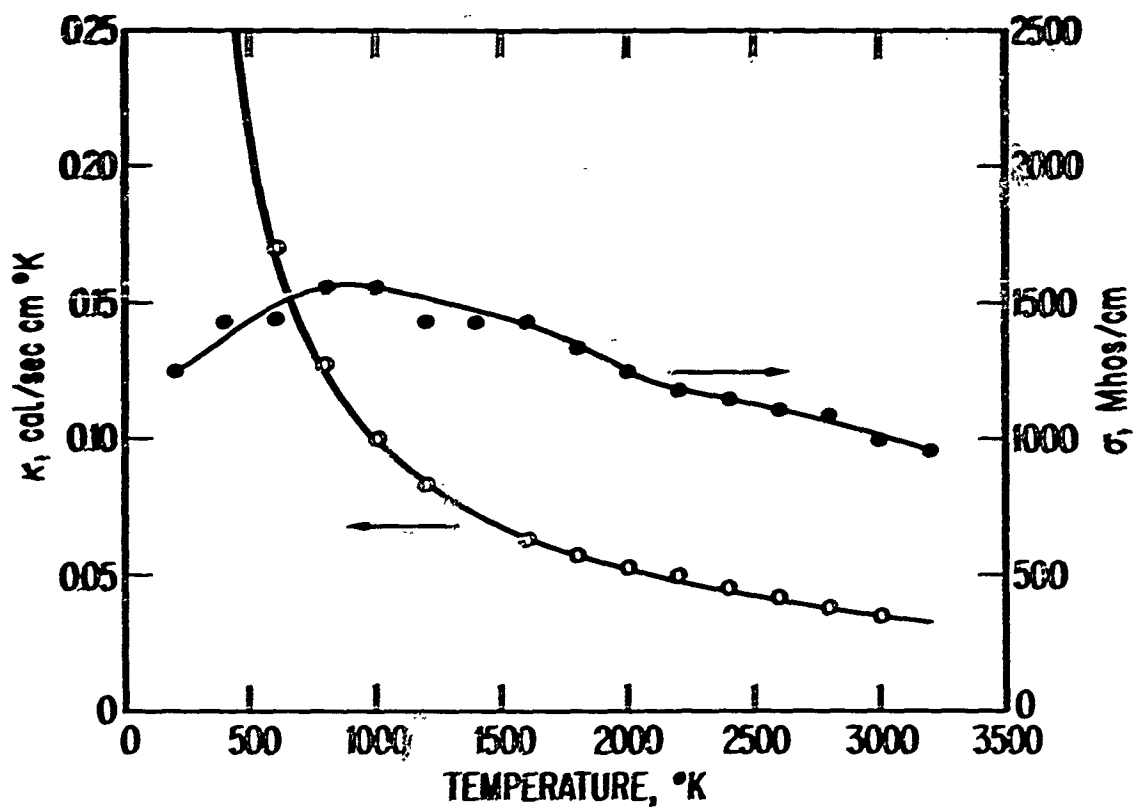


Figure II-1. Variations of thermal conductivity κ and electrical conductivity σ with temperature for ATJ graphite

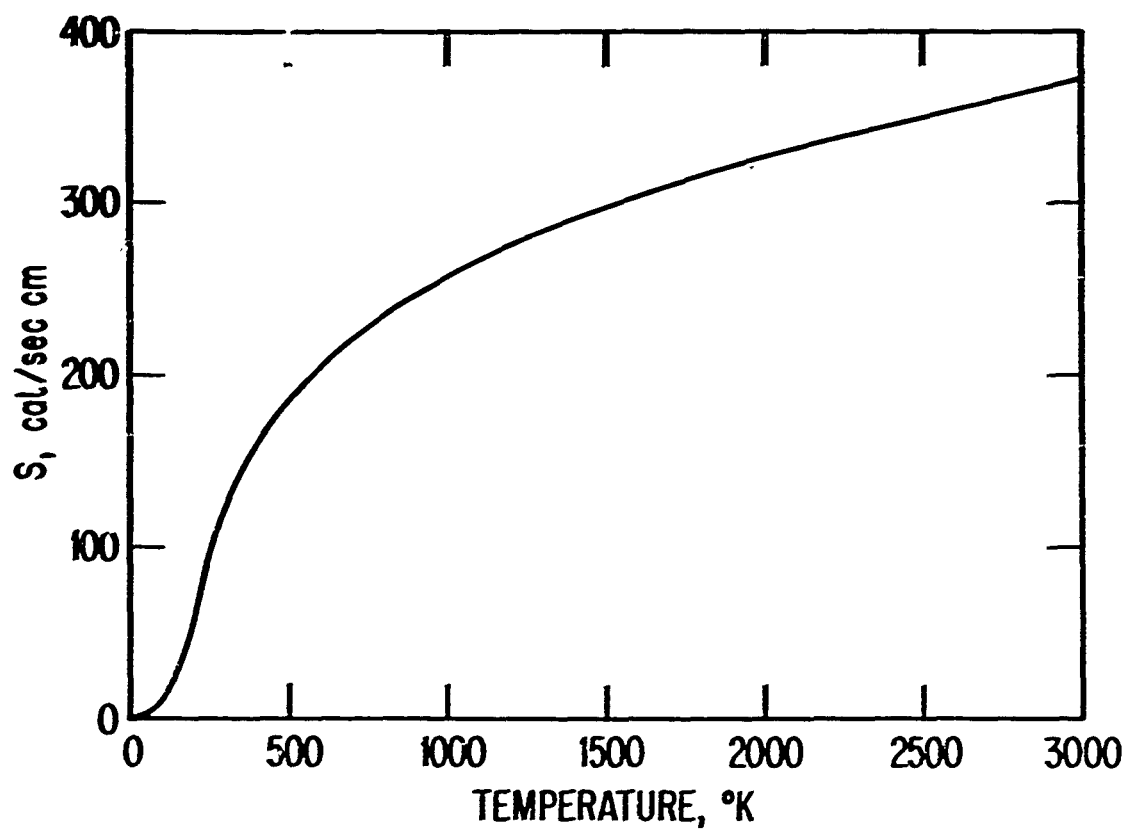


Figure II-2. Heat conduction potential of ATJ graphite

The constant C is determined at the outer boundary r_2 where $x = 1$ and

$\frac{dS}{dx} = \left(\frac{dS}{dx}\right)_2$, so that

$$C = \left(\frac{dS}{dx}\right)_2 + \frac{r_2^2 \bar{\sigma} E_2^2}{2q+2} \quad (34)$$

Here, the heat flux is balanced by gray body radiation from the surface.

Therefore

$$\frac{1}{r_2} \left(\frac{dS}{dx}\right)_2 = -\epsilon \Sigma T_2^4 \equiv -f(S_2) \quad (35)$$

The second integration of Eq. (33) yields

$$S + \frac{r_2^2 \bar{\sigma} E_2^2}{(2q+2)^2} x^{2q+2} = C \ln x + C' \quad (36)$$

After evaluation of C' at the inner boundary r_i , where $x = x_i$ and $S = S_i$, Eq. (36) can be written

$$S = S_i + C \ln \frac{x}{x_i} - \frac{r_2^2 \bar{\sigma} E_2^2}{(2q+2)^2} \left(x^{2q+2} - x_i^{2q+2} \right) \quad (37)$$

or, when using Eqs. (34) and (35) and considering that the power dissipated per unit length is

$$\frac{P}{l} = \frac{2\pi r_2^2 \bar{\sigma} E_2^2}{2q+2} \left(1 - x_i^{2q+2} \right) \quad (38)$$

$$S = S_i - r_2 f(S_2) \ln \frac{x}{x_i} + \frac{P}{2\pi l} (1 - x_i^{2q+2})^{-1} \times$$

$$\left(\ln \frac{x}{x_i} - \frac{x^{2q+2} - x_i^{2q+2}}{2q+2} \right) \quad (39)$$

The function $f(S_2)$ in Eq. (35) has been evaluated for $\epsilon = 0.85$ and is plotted in Fig. II-3. Writing Eq. (39) for the outer boundary $x = l$ yields an implicit equation for S_2 that can be evaluated with the aid of Fig. II-3 so that $f(S_2)$ also is determined. $S(x)$ can then be calculated from Eq. (39). $T(x)$ finally can be obtained from the function $S(T)$ in Fig. II-2.

Some examples of temperature distributions obtained by this method are shown in Figs. II-4 and II-5. Figure II-4 shows the effect of frequency for $\frac{P}{l} = 1$ kW/cm and an inner surface temperature of 1000°C at $r_i = 0.4$ cm. These conditions represent approximately those in the early tests with specimen (a) in Fig. 2. Results for $f = 1.7$ MHz are shown in Fig. II-5; $T_i = 273^\circ\text{K}$, $P/l = 3, 4$ and 5 kW/cm, $r_i = 0.4$ and 0.63 cm are values that represent conditions in the later tests. The curve for $\frac{P}{l} = 4$ kW/cm and $r_i = 0.4$ cm, in particular, is believed to represent closely the conditions at which fracture occurred, although a steady state may not have been reached in every test. The mean gradient is $\sim 1300^\circ\text{K/cm}$. It is remarkable that all curves show a nearly linear distribution, although the heat flux is strongly convergent. This is caused by the strong increase in thermal conductivity toward the cool inner surface, which compensates for the effect of convergence. If this result is generally true and if it holds in particular also for ATJ-S graphite, the situation is greatly simplified. Then the value of the mean gradient, which is determined experimentally from the temperature difference between inner and outer surfaces, also approximates that of the local gradient at any radial position and makes detailed measurements or calculations unnecessary.

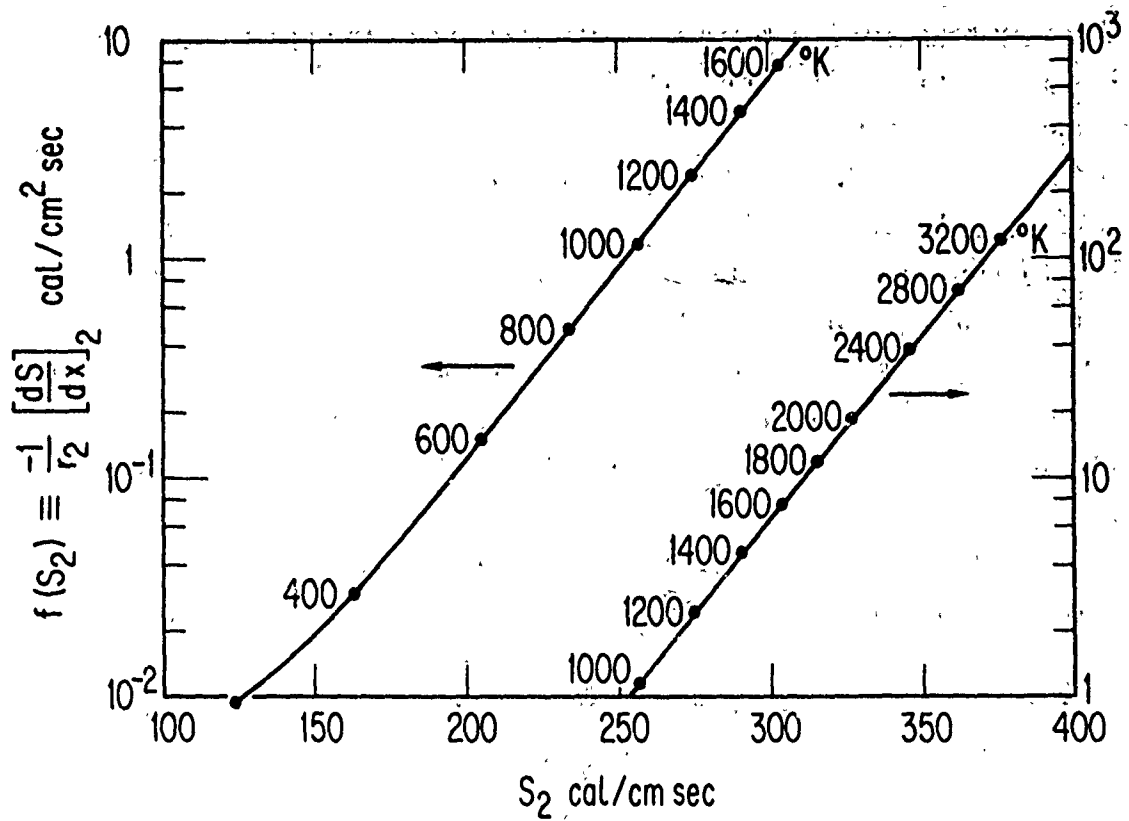


Figure II-3. Radiation flux vs heat conduction potential of ATJ graphite

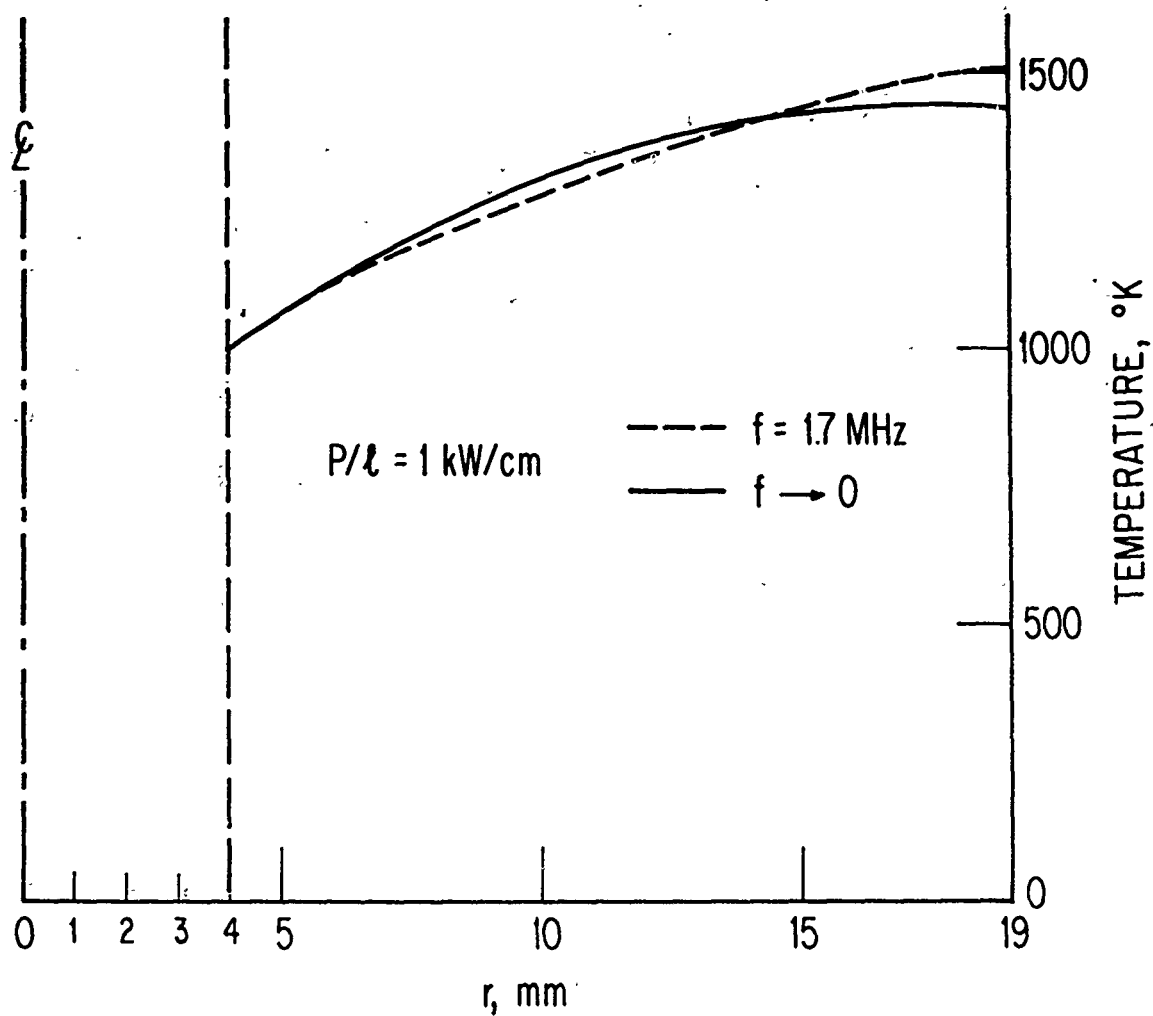


Figure II-4. Calculated temperature distributions in induction-heated ATJ graphite cylinder; low input $\frac{P}{l} = 1 \text{ kW/cm}$, ---- $f = 1.7 \text{ MHz}$, — $f = \rightarrow 0$

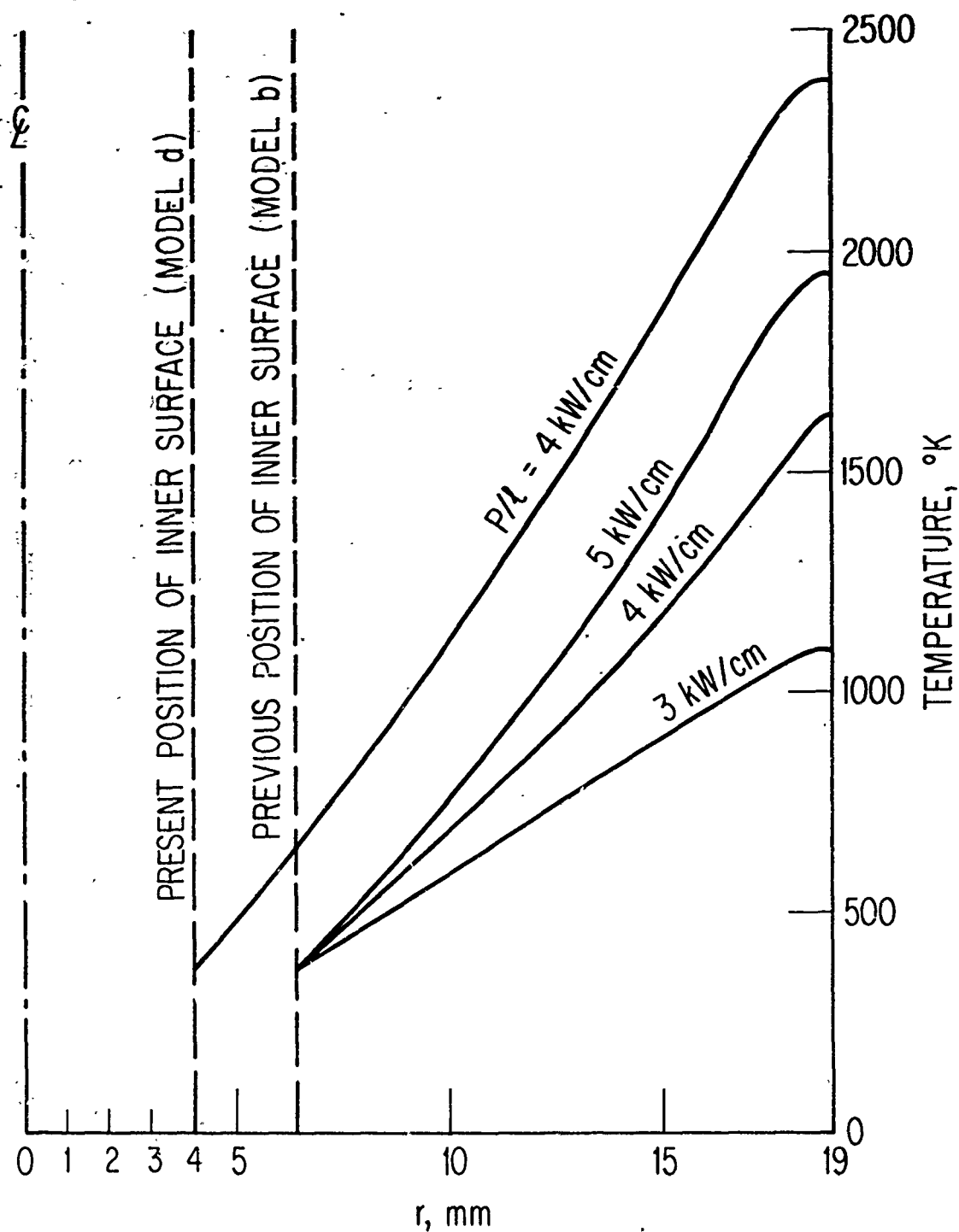


Figure II-5. Calculated temperature distributions in induction-heated ATJ graphite cylinder; high input, $f = 1.7 \text{ MHz}$. Inner surface temperature 373°K ; outer surface temperature determined by radiation equilibrium